Band gap narrowing models tested on low recombination phosphorus laser doped silicon

Morris Dahlinger[a] and Kai Carstens
Institute for Photovoltaics (ipv) and Research Center SCoPE, University of Stuttgart, Pfaffenwaldring 47, 70569 Stuttgart, Germany

(Received 15 August 2016; accepted 5 October 2016; published online 19 October 2016)

This manuscript discusses bandgap narrowing models for highly phosphorus doped silicon. We simulate the recombination current pre-factor $J_{0,phos}$ in PC1Dmod 6.2 of measured doping profiles and apply the theoretical band gap narrowing model of Schenk [J. Appl. Phys. **84**, 3684 (1998)] and an empirical band gap narrowing model of Yan and Cuevas [J. Appl. Phys. **114**, 044508 (2013)]. The recombination current pre-factor of unpassivated and passivated samples measured by the photo conductance measurement and simulated $J_{0,phos}$ agrees well, when the band gap narrowing model of Yan and Cuevas is applied. With the band gap narrowing model of Schenk, the simulation cannot reproduce the measured $J_{0,phos}$. Furthermore, the recombination current pre-factor of our phosphorus laser doped silicon samples are comparable with furnace diffused samples. There is no indication of recombination active defects, thus no laser induced defects in the diffused volume. *Published by AIP Publishing*. [http://dx.doi.org/10.1063/1.4964950]

I. INTRODUCTION

There is an ongoing discussion on the bandgap narrowing (BGN) models for the simulation of highly doped regions in silicon devices.[1,2] High doping concentration causes band gap narrowing effects, which tend to increase the intrinsic charge carrier concentration n_i,[3] thus increases recombination. The theoretical BGN model of Schenk[4] in conjunction with Fermi-Dirac (FD) statistics and an intrinsic charge carrier density $n_i = 9.65 \times 10^9\,\mathrm{cm}^{-3}$ at a temperature $T = 300\,\mathrm{K}$ is widely spread in common simulation tools such as Sentaurus TCAD,[5] EDNA2,[6,7] and PC1Dmod 6.2.[8] Recently, Yan and Cuevas found that their experimentally measured recombination current pre-factor $J_{0,phos}$ of metalized (unpassivated) samples cannot be reproduced by simulation using Schenk's BGN model. Consequently, they suggested an empirical BGN model based on their experimental data,[1] with parametrization for the use in conjunction with Fermi-Dirac and the Boltzmann statistics. Unfortunately, there is still no obvious decision on which of the two models is correct.

Our experiment supports the BGN model of Yan and Cuevas. We measure the recombination current pre-factor $J_{0,phos}$ by photo conductance (PC) measurement and simulate $J_{0,phos}$ using doping profiles, measured by electrochemical capacitance-voltage (ECV), and a modified version PC1Dmod 6.2[8] of the popular simulation tool PC1D 5.9.[9] The measured $J_{0,phos}$ cannot be reproduced in simulation, neither for passivated nor unpassivated samples, if the BGN model of Schenk is applied.

There is a laser doping step included in our sample's preparation. Laser doping of silicon is often linked with the introduction of recombination centers (defects or impurities).[10–13] However, we show that there is no indication of laser induced recombination centers. Our measured $J_{0,phos}$ of laser doped samples are comparable with furnace diffused phosphorus doped silicon in the investigated range of sheet resistances R_{sh}. The presented process includes all steps which are also used in our laser doped fine line back contact solar cells[14,15] that achieved an efficiency of $\eta = 23.2\%$.[16,17]

II. EXPERIMENTAL METHODS

To evaluate the recombination current pre-factor $J_{0,phos}$, we prepare symmetrically phosphorus laser doped samples for PC measurement using the following steps:

1. n-type CZ wafer
2. KOH surface polishing
3. HCl + HF cleaning
4. $POCl_3$ diffusion
5. Laser doping
6. RCA cleaning
7. Thermal oxidation
8. PC measurement
9. SiO_2 removal
10. PC measurement
11. Four-point-probe
12. HCl + HF cleaning
13. PECVD a-Si deposition
14. Hot plate annealing
15. PC measurement
16. ECV

A high lifetime n-type Czochralski (CZ) 6 in. mono crystalline silicon wafer with a specific resistance of $\rho \approx 2\,\Omega\,\mathrm{cm}$ is polished on both sides in potassium hydroxide solution. After cleaning in hydrochloric acid (HCl) and hydrofluoric acid (HF) solutions, we apply a phosphoryl chloride ($POCl_3$) furnace diffusion in a three zone *Centrotherm* open tube furnace. A shallow phosphorus profile forms at the wafer surface, and a phosphor silicate glass

[a]Electronic mail: morris.dahlinger@ipv.uni-stuttgart.de

(PSG) grows. The PSG serves as a dopant source for the following laser doping step. We adjust the phosphorus concentration in the PSG, thus the dopant source for the laser doping, by changing the diffusion recipe, in particular, the $POCl_3$ flow.[18] The doping profiles are adjustable in a wide range of surface concentration $c_{P,surf}$ and depth z, and thus the sheet resistances R_{sh} vary as described in Ref. 18 and in Sec. III. For the evaluation of the $J_{0,phos}$, we scan the front and the rear side full area with our line shaped nanosecond pulsed laser beam of the wavelength $\lambda = 532\,\text{nm}$. The laser beam is Gaussian shaped in the short axis with a full width at half maximum of $w_x \approx 10\,\mu\text{m}$ and a homogeneous intensity distribution in the long axis with a length of $w_y \approx 800\,\mu\text{m}$. We scan the areas of $4 \times 4\,\text{cm}^2$ with varied laser pulse energy densities H with an offset between the succeeding pulses of $\Delta x = 3.2\,\mu\text{m}$ in x-direction and a y-offset of $800\,\mu\text{m}$. The wafer surface melts, where the laser pulse irradiates the sample. The phosphorus atoms diffuse into the liquid silicon. Shortly after the laser pulse terminates, the liquid silicon starts to solidify and recrystallize epitaxially and is then doped with phosphorus. After laser doping of both sides and subsequent RCA cleaning, dry thermal oxidation at a temperature $T = 1000\,^\circ\text{C}$ drives in the dopant atoms, and the grown $d_{SiO_2} = 14\,\text{nm}$ thick SiO_2 layer passivates the surfaces. At this stage, no special hydrogenation step is applied. Subsequently, we measure the injection dependent minority charge carrier lifetimes with a *Sinton WCT-120* tester in a generalized mode.[19] Diluted HF acid removes the SiO_2 passivation layer, before the second PC measurement of the same unpassivated samples. After wet chemical cleaning in subsequent HCl and HF solutions, we deposit a $t_{a-Si:H} = 30\,\text{nm}$ thick hydrogenated amorphous silicon (a-Si:H) layer by plasma enhanced chemical vapor deposition (PECVD) in an *Oxford Plasmalab 100* parallel plate reactor on both sides of the wafer. An annealing step on a hotplate for $t = 5\,\text{min}$ at $T = 350\,^\circ\text{C}$ increases the surface passivation significantly.[20] PC measures again the recombination current pre-factor of the now a-Si:H passivated samples. Finally, ECV profiling measures the electrically active phosphorus doping profile. The 30 nm thick a-Si:H layer is subtracted from the depths of the profiles. The absolute phosphorus doping concentration c_P is then scaled to match the sheet resistances, measured by a four-point-probe on separate wafers. This way, we account for inconstant contact area during the ECV measurement.

The advantage of using high quality n-type wafers for PC measurements lies in the good availability of high bulk lifetime wafers, which only show insignificant injection dependent Shockley-Read-Hall (SRH) recombination. For this wafers, the injection range for accurate recombination current pre-factor evaluation in the lifetime curves is increased. We extract the recombination current pre-factor using Equation (8) from Kimmerle *et al.*[21] for a temperature $T = 300\,\text{K}$ and an intrinsic charge carrier density $n_i = 9.65 \times 10^9\,\text{cm}^{-3}$, in an injection range $4 \times 10^{15}\,\text{cm}^{-3} \le \Delta n \le 1 \times 10^{16}\,\text{cm}^{-3}$. This approach accounts for SRH-recombination and charge carrier diffusion, which is necessary, especially, for samples with highly recombination active (unpassivated, metalized) surfaces. Without accounting for charge carrier diffusion, the $J_{0,phos}$ will likely be underestimated. The disadvantage of using $\rho = 2\,\Omega\,\text{cm}$ n-type wafers is that the wafer doping and the diffused region are of the same kind. Therefore, the resistivity of the wafer is included in an inductive coil or four-point-probe sheet resistance measurement, which significantly increases the uncertainty in R_{sh}. For sheet resistance measurement, we simultaneously process p-type wafers with $\rho = 3\,\Omega\,\text{cm}$, with the same parameters as the n-type PC samples. The R_{sh} for each parameter set ($POCl_3$ flow and laser pulse energy density H) are averaged from the areas distributed on two wafers. We measure the R_{sh}, the $J_{0,phos}$, and the doping profiles of ten samples, manufactured with varied $POCl_3$ flow of $100\,\text{sccm} \le f_{POCl_3} \le 200\,\text{sccm}$ and varied laser pulse energy density of $2.5\,\text{J/cm}^2 \le H \le 4.3\,\text{J/cm}^2$. Section III exemplarily shows the influence of the $POCl_3$ flow and the laser pulse energy density H on the doping profile for five profiles.

III. RESULTS

A. Doping profiles

Figure 1(a) shows the phosphorus doping profiles for varied laser pulse energy densities H. The $POCl_3$ flow $f_{POCl_3} = 150\,\text{sccm}$ is constant, hence the composition of the PSG does not change. The profiles are labeled with their corresponding pulse energy density H and measured sheet resistance R_{sh}. The surface concentration is almost constant $c_{P,surf} \approx 4 \times 10^{19}\,\text{cm}^{-3}$ for the three profiles. The depth increases with increasing H from $H = 2.5\,\text{J/cm}^2$ to $H = 4.3\,\text{J/cm}^2$. The final doping profiles arise from both the initial doping profile after laser induced liquid phase diffusion and the additional solid phase diffusion during the thermal oxidation. It is just a

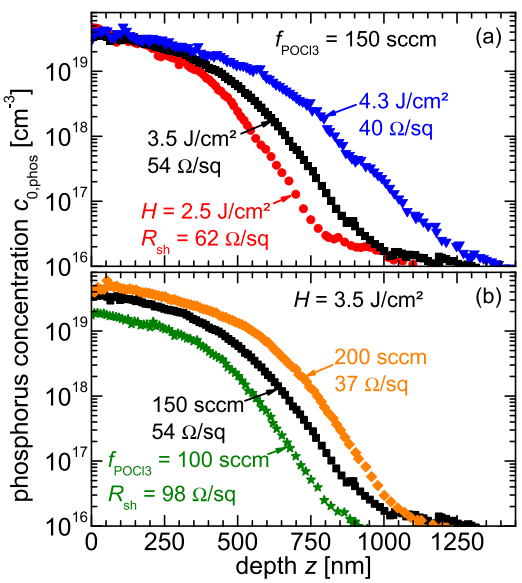

FIG. 1. Phosphorus doping profiles after laser doping from PSG and subsequent thermal oxidation (drive-in) measured by ECV. (a) For constant $POCl_3$ flow $f_{POCl_3} = 150$ sccm, the depth increases with increasing laser pulse energy density H. (b) With constant $H = 3.5\,\text{J/cm}^2$ and increasing $POCl_3$ flow f_{POCl_3}, the shape of the doping profiles stay basically the same, but shift to higher surface concentrations. The R_{sh} are measured separately on 3 Ω cm doped p-type wafers by four point probe measurement.

coincidence that the surface concentrations for this three profiles are the same. Further reduced pulse energy densities or a longer drive-in would result in different profile shapes and varied surface concentrations. Utilizing the laser doped profiles before oxidation as initial profiles would enable to simulate the solid phase diffusion during the oxidation. Unfortunately, doping profiles before thermal oxidation are not available. Nevertheless, the profiles show that the laser pulse energy density H adjusts the depth of the profile.

Figure 1(b) shows the doping profiles of samples irradiated with a constant laser pulse energy density $H = 3.5\,\mathrm{J/cm^2}$ and varied $POCl_3$ flow f_{POCl_3}. The shape of these profiles stays basically the same, but depending on the $POCl_3$ flow f_{POCl_3}, they shift in concentration c_P. A reduced $POCl_3$ flow depletes the phosphorus concentration in the PSG; hence, the dopant source is limited. Consequently, the phosphorus concentration is reduced, and the sheet resistance R_{sh} increases.

Figures 1(a) and 1(b) show that laser doping in conjunction with furnace grown PSG as dopant source and subsequent thermal oxidation enables us to tailor the sheet resistance R_{sh} by adjusting the doping profile in depth and surface concentration. Similar results were found by our group for laser doping with sputtered boron precursor.[22]

B. Recombination pre-factor

Figure 2 shows the recombination current pre-factor depending on the R_{sh} in the unpassivated state, measured by PC. As the doping is reduced, the R_{sh} increases and the minority charge carriers reach the highly recombination active surface more easily, recombine there, and hence $J_{0,phos}$ increases. We compare the results with the $J_{0,phos}$ values from Ref. 23, Figure 8 and Ref. 1, Figure 4. Although our experiment differs in base doping of the used wafers, phosphorus diffusion profiles, surface condition, and the method for the $J_{0,phos}$ evaluation, the recombination current pre-factors agree well.

To further investigate the recombination in the doped volumes, we simulate the recombination current pre-factor for a temperature $T = 300\,\mathrm{K}$ using PC1Dmod 6.2.[8] We use

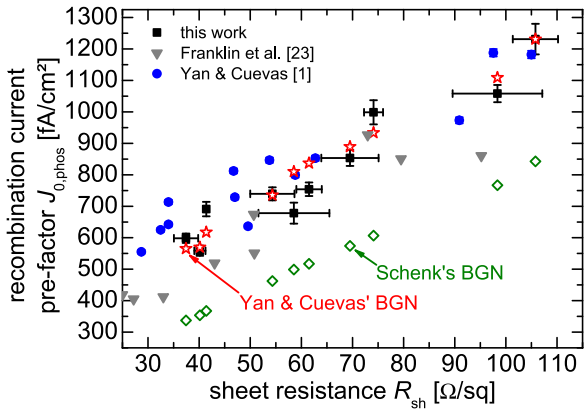

FIG. 2. The recombination current pre-factor $J_{0,phos}$ of unpassivated samples measured by PC and modeled using the doping profiles and PC1Dmod 6.2. The modeling using the BGN model of Yan and Cuevas reproduces the measured $J_{0,phos}$. The measured $J_{0,phos}$ values agree well with $J_{0,phos}$ of furnace diffused samples published by Yan and Cuevas and Franklin *et al.*

TABLE I. Models used in PC1Dmod 6.2 simulation, described with the same terminology as in the program.

Description	Model
Carrier statistics	Fermi-Dirac (FD)
Band gap	Green1990 (Ref. 24)
Density of states	Haug2014 (Ref. 25)
Mobility model	Klaassen1992 (Ref. 26)
Intrinsic recombination	Richter2012 (Ref. 27)
Incomplete ionization	100% ionization (PC1D5)
Temperature	$T = 300\,\mathrm{K}$
Intrinsic carrier concentration	$n_i = 9.65 \times 10^9\,\mathrm{cm^{-3}}$

the theoretical BGN model developed by Schenk[4] and the empirical BGN model of Yan and Cuevas.[1] The need for Fermi-Dirac statistics instead of the Boltzmann statistics for the accurate modeling of highly doped silicon using the BGN model of Yan and Cuevas has been thoroughly demonstrated in Ref. 2; thus, we apply Fermi-Dirac statistics in this work. Table I lists the used models.

We use the doping profiles measured by ECV and repeat the simulation of the $J_{0,phos}$ in PC1Dmod 6.2 with a surface recombination velocity of $S_p = 3 \times 10^6\,\mathrm{cm/s}$,[1,28] as is representative for the unpassivated surface and $S_p = 0\,\mathrm{cm/s}$ for perfect passivation (no SRH-recombination in the diffused volume nor at the surface). With Schenk's BGN model, the simulation cannot reproduce the measured $J_{0,phos}$, but simulation with the Yan and Cuevas BGN model agrees well with the measured $J_{0,phos}$.

Figure 3 shows the $J_{0,phos}$ values, measured by PC, of the same set of samples passivated with SiO_2 and a-Si:H. Since the samples of the shown $J_{0,phos}$ are processed with varied f_{POCl_3} and H, we see the well-known tendency that deeper diffusion profiles yield a slightly lower $J_{0,phos}$ compared to shallow profiles with the same R_{sh}. Beyond this observation, we do not see unexpectedly high $J_{0,phos}$ for any

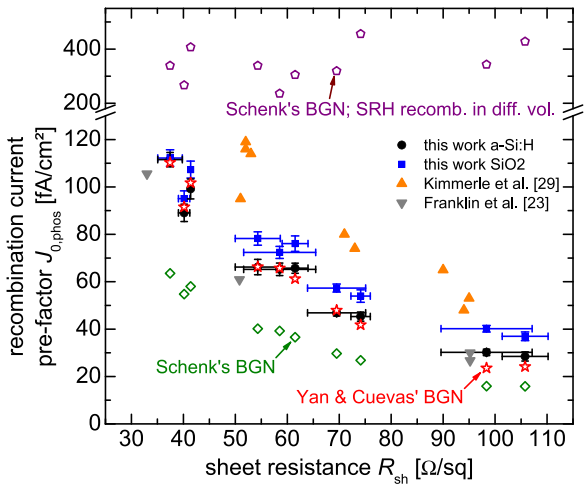

FIG. 3. The recombination current pre-factor $J_{0,phos}$ of passivated samples measured by PC and modeled using the doping profiles and PC1Dmod 6.2. Simulation using the BGN model of Yan and Cuevas reproduces the measured $J_{0,phos}$ well. Our $J_{0,phos}$ values agree well with furnace diffused phosphorus silicon from Kimmerle *et al.*[29] and Franklin *et al.*[23] With Schenk's BGN model, the measured $J_{0,phos}$ cannot be reproduced, even with introduction of SRH recombination in the diffused volume.

parameter combination. Thus for clarity, we desist from labeling the individual data points. For comparison, Figure 3 shows the $J_{0,phos}$ values of phosphorus furnace diffused SiO_2 passivated samples from Ref. 23, Figure 8 and Ref. 29, Figure 4(b). The $J_{0,phos}$ of our samples increase with decreasing R_{sh} due to Auger-recombination. The SiO_2 passivated samples show a 5 to 10 fA/cm^2 higher $J_{0,phos}$ than with a-Si:H passivation. Besides the well passivated surface, the hydrogen released during the a-Si:H deposition and post annealing might passivate defects within the silicon volume. Our $J_{0,phos}$ agrees well with the data from Ref. 23, Figure 8; original $J_{0,phos}$ data from Ref. 23 for $T = 298.15$ K are scaled to $T = 300$ K using the relation,

$$\frac{J_{0,298.15K}}{n_{i,298.15K}^2} = \frac{J_{0,300K}}{n_{i,300K}^2}. \quad (1)$$

Compared to the $J_{0,phos}$ from Kimmerle *et al.*,[29] we achieve lower $J_{0,phos}$ values for SiO_2 and a-Si:H passivation. Both experimental approaches are similar to ours, despite in Ref. 29 exclusively furnace diffusion is used while we have a laser irradiation step included.

Furthermore, Figure 3 shows the simulated $J_{0,phos}$ from the measured dopant profiles with assumed perfect surface passivation $S_p = 0$ cm/s. With Schenk's BGN model, significantly lowered $J_{0,phos}$ compared to the measured $J_{0,phos}$ is simulated. With the Yan and Cuevas BGN model, the simulated $J_{0,phos}$ agrees well with the measured $J_{0,phos}$, but with the tendency of the simulated $J_{0,phos}$ exceeding the measured ones for low R_{sh}, which would require a negative S_p. We repeat the simulation applying the upper and lower values of the standard deviation of the parametrization (band gap slope $A = 42$ meV $\pm$ 3 meV),[1] and find our measured $J_{0,phos}$ are fairly within this uncertainty. Thus, we do not propose a new parametrization.

IV. DISCUSSION ON LASER INDUCED DEFECTS

Our measured $J_{0,phos}$ coincides well with exclusively furnace diffused phosphorus doping profiles reported in Ref. 1 and also in passivated state from Ref. 23. The simulation using the BGN model of Yan and Cuevas reproduces our measured $J_{0,phos}$ well without any SRH-recombination in the diffused volume, as shown in Figure 2. If the BGN model of Yan and Cuevas is considered valid, one would conclude that there are no laser induced defects. On the other hand, to reproduce the $J_{0,phos}$ in the unpassivated state with Schenk's BGN model either a surface recombination velocity that significantly exceeds the thermal velocity (which is impossible) or SRH lifetimes $\tau_{SRH,phos}$ in a range of few ten nanoseconds in the diffused volume are required. Since laser irradiation of silicon is aspersed to introduce contamination and defects,[10–13] we show that Schenk's BGN model cannot reproduce our experimental results even with additional SRH-recombination in the diffused volume.

The modeling of the dopant profiles including SRH recombination requires many unknowns like energetic and spatial defect distribution, density and capture cross sections for electrons and holes. Furthermore, the recombination current pre-factor depends on the junction voltage V_j, which is required for the numerical simulation. Still, we want to provide the results of a simplified simulation using the tool EDNA2,[6] provided by the website: www.pvlighthouse.com.au, where we use basically the same models as listed in Table I in conjunction with Schenk's BGN model. The junction voltage is set to $V_j = 0.68$ V, which represents the lower limit of the implied open circuit voltage $V_{oc,impl}$ in the $J_{0,phos}$ evaluation range in the PC measurement. Furthermore, we assume a single defect level in the middle of the band gap E_t–$E_i = 0$ meV, and the SRH lifetime of electrons and holes equal $\tau_{SRH} = \tau_e = \tau_h$ in the diffused region. We simulate the unpassivated state ($S_p = 3 \times 10^6$ cm/s) and decrease τ_{SRH} in the diffused volume till the simulated $J_{0,phos}$ matches the measured one. Subsequently, we set $S_p = 0$ cm/s and simulate the perfectly passivated state with the same τ_{SRH} and extract the $J_{0,phos}$.

Figure 3 additionally shows the $J_{0,phos}$ simulated using Schenk's BGN model with $S_p = 0$ cm/s and the determined τ_{SRH} in the diffused volume. With the required τ_{SRH} to match the $J_{0,phos}$ in the unpassivated state in conjunction with Schenk's BGN model, the simulation cannot reproduce the measured $J_{0,phos}$ of the passivated samples. Since the $J_{0,phos}$ of SiO_2 passivated samples is measured prior to the unpassivated samples (SiO_2 stripped), the assumption is fulfilled that neither curing (hydrogen passivation) nor introduction of defects in the volume occurs between the measurements. The simulated $J_{0,phos}$ including τ_{SRH} is in the range of 250 fA/cm^2 to 500 fA/cm^2 for all samples and does not show a visible trend. Consequently, the low measured $J_{0,phos}$ does not allow for significant SRH recombination in the diffused region; hence, the laser irradiated samples do not suffer from high recombination, if the proposed process sequence is used.

V. CONCLUSION

Our work has shown that the $J_{0,phos}$ of phosphorus laser doped silicon and subsequent thermal oxidation are reproduced by simulation using measured doping profiles and the BGN model of Yan and Cuevas. The recombination current prefactor in unpassivated and passivated states, measured by PC, are comparable to reported $J_{0,phos}$ of furnace diffused phosphorus surfaces. There is no indication of laser induced recombination active defects within the investigated parameter range, when the proposed process flow is met. Simulated $J_{0,phos}$ using ECV measured doping profiles in conjunction with Schenk's BGN model cannot reproduce our measured $J_{0,phos}$. With the band gap narrowing model of Yan and Cuevas, the modeled $J_{0,phos}$ agrees well. Therefore, we recommend using the BGN model of Yan and Cuevas in device simulation.

ACKNOWLEDGMENTS

The authors thank L. Beisel, H. Moldenhauer, B. Lutz, and B. Winter for the technological support, as well as C. Sämann, E. Hoffmann, J. R. Köhler, R. Zapf-Gottwick, and J. H. Werner for carefully reading the manuscript and steady support. Furthermore, we thank the ISC Konstanz, Germany, in particular, Christoph Peter for the ECV measurements.

This work was funded by German Federal Ministry of Economics and Technology (BMWi) project No. 0325714A.

[1]D. Yan and A. Cuevas, J. Appl. Phys. **114**, 044508 (2013).
[2]A. Kimmerle, J. Greulich, H. Haug, and A. Wolf, J. Appl. Phys. **119**, 025708 (2016).
[3]R. J. Van Overstraeten and R. P. Mertens, Solid State Electron. **30**, 1077 (1987).
[4]A. Schenk, J. Appl. Phys. **84**, 3684 (1998).
[5]Synopsis, Sentaurus Device User Guide Version, 2009, c-2009.06.
[6]R. Girisch, R. Mertens, and R. De Keersmaecker, IEEE Trans. Electron Devices **35**, 203 (1988).
[7]K. McIntosh, P. Altermatt, T. Ratcliff, K. Fong, L. Black, S. Baker-Finch, and M. Abbott, in *28th European Photovoltaics Science and Engineering Conference* (2013), pp. 1672–1679.
[8]H. Haug and J. Greulich, Energy Procedia **92**, 60–68 (2016).
[9]D. A. Clugston and P. A. Basore, in *26th IEEE Photovoltaic Specialists Conference* (1997), pp. 207–210.
[10]Z. Hameiri, T. Puzzer, S. A. B. Mai, L. and, and S. R. Wenham, Prog. Photovoltaics **19**, 391 (2011).
[11]M. F. Ametowobla, "Characterization of a laser doping process for crystalline silicon solar cells," Ph.D. thesis (Universität Stuttgart, Stuttgart, 2010).
[12]R. T. Young, R. F. Wood, J. Narayan, C. W. White, and W. H. Christie, IEEE Trans. Electron Devices **27**, 807 (1980).
[13]K. Ohmer, Y. Weng, J. R. Köhler, H. P. Strunk, and J. H. Werner, IEEE J. Photovoltaics **1**, 183 (2011).
[14]M. Dahlinger, B. Bazer-Bachi, T. C. Röder, J. R. Köhler, R. Zapf-Gottwick, and J. H. Werner, Energy Procedia **38**, 250 (2013).
[15]K. Carstens, M. Dahlinger, E. Hoffmann, J. R. Köhler, R. Zapf-Gottwick, and J. H. Werner, Energy Procedia **77**, 779 (2015).
[16]M. Dahlinger, B. Bazer-Bachi, T. C. Röder, J. R. Köhler, R. Zapf-Gottwick, and J. H. Werner, IEEE J. Photovoltaics **5**, 812 (2015).
[17]M. Dahlinger, K. Carstens, E. Hoffmann, R. Zapf-Gottwick, and J. Werner, "Laser Processed Back Contact Solar Cells: Fabrication, Characterization and Modeling" (to be published).
[18]M. Dahlinger and K. Carstens, Energy Procedia **92**, 450–456 (2016).
[19]H. Nagel, C. Berge, and A. G. Aberle, J. Appl. Phys. **86**, 6218 (1999).
[20]K. Carstens and M. Dahlinger, J. Appl. Phys. **119**, 185303 (2016).
[21]A. Kimmerle, J. Greulich, and A. Wolf, Sol. Energy Mater. Sol. Cells **142**, 116 (2015).
[22]M. Dahlinger, S. Eisele, J. R. Köhler, and J. Werner, in *26th European Photovoltaics Solar Energy Conference* (2011), pp. 1152–1154.
[23]E. Franklin, K. Fong, K. McIntosh, A. Fell, A. Blakers, T. Kho, D. Walter, D. Wang, N. Zin, M. Stocks, E.-C. Wang, N. Grant, Y. Wan, Y. Yang, X. Zhang, Z. Feng, and P. J. Verlinden, Prog. Photovoltaic **24**, 411 (2016).
[24]M. A. Green, J. Appl. Phys. **67**, 2944 (1990).
[25]H. Haug, A. Kimmerle, J. Greulich, A. Wolf, and E. Stensrud Marstein, Sol. Energy Mater. Sol. Cells **131**, 30 (2014).
[26]D. Klaassen, Solid State Electron. **35**, 953 (1992).
[27]A. Richter, S. W. Glunz, F. Werner, J. Schmidt, and A. Cuevas, Phys. Rev. B **86**, 165202 (2012).
[28]A. Cuevas, P. A. Basore, G. Giroult-Matlakowski, and C. Dubois, J. Appl. Phys. **80**, 3370 (1996).
[29]A. Kimmerle, M. Momtazur Rahman, S. Werner, S. Mack, A. Wolf, A. Richter, and H. Haug, J. Appl. Phys. **119**, 025706 (2016).